Journal of Engineering Science and Technology
Vol. 6, No. 6 (2011) 745 - 768

FLOW BEHIND BLUFF BODIES IN SIDE-BY-SIDE ARRANGEMENT

PUNEESHWAR LAL VERMA, M. GOVARDHAN*

Department of Mechanical Engineering,
Indian Institute of Technology Madras, Chennai 600 036, India
*Corresponding Author: gova@iitm.ac.in

Abstract

The present investigation deals with the shedding of vortices and flow interference between two circular cylinders in a side-by-side arrangement. Simulations are carried out using commercial Computational Fluid Dynamics (CFD) code FLUENT-6.2. The flow field around the cylinders is modeled in two-dimensions with the axis of the cylinder perpendicular to the direction of flow. The cylinder is modeled as a circle and a square flow domain is created around the cylinder. The calculations are carried out on a quadrilateral mesh. The simulations are performed for a Reynolds number of 200. The mesh is finer close to the cylinder wall in order to have a better description of the boundary layer. Contours of vorticity, variation of lift and drag coefficients, force time histories are presented. A mean repulsive lift force exists between the cylinders and the lift force steadily decreases with increasing length to diameter ratio. For length to diameter ratio $\leq$ 2.0, flopping phenomenon is observed whereas for length to diameter ratio > 2.0, the lift fluctuation is synchronized and is in anti-phase. The results of the present work show that the drag coefficient is slightly higher for length to diameter ratio of 2.0. Beyond this ratio, the drag coefficient on either cylinder falls. For length to diameter ratio of 3.0 and 4.0, the power spectrum estimation of the lift coefficient shows a very distinctive peak at Strouhal number of 0.21.

Keywords: Bluff bodies, Cylinders, Numerical simulation, Vortices, Interference, Lift, Drag, Flow separation.

1. Introduction

When a fluid flows over a body separation may occur depending on its shape and other parameters. The flow separation can cause periodic shedding of vortices from the body. The vortex shedding under certain conditions may have important

Nomenclatures

C_{D1}	Drag coefficient of upstream cylinder or upper cylinder
C_{D2}	Drag coefficient of downstream cylinder or lower cylinder
C_{L1}	Lift coefficient of upstream cylinder or upper cylinder
C_{L2}	Lift coefficient of downstream cylinder or lower cylinder
D	Diameter of cylinder, m
	Drag force, N
F	Force, N
f	Vortex shedding frequency, s^{-1}
g	Gravitational constant, m/s^2
I	Unit tensor
L	Gap between two cylinders, m
	Lift force, N
p	Pressure, N/m^2
Re	Reynolds number
S_M	Momentum of force, $kg/m^2\ s^2$
S_{t1}	Strouhal number of upper cylinder or upstream cylinder
S_{t2}	Strouhal number of lower cylinder or downstream cylinder
t	Time, s
U_o	Free stream velocity, m/s
v	Velocity in y direction, m/s

Greek Symbols

μ	Dynamic viscosity of fluid, kg/m.s
ν	Kinematic viscosity of fluid, m^2/s
τ	Stress tensor

practical consequences such as noise, vibration of structure or even structural failure [1]. The control of such phenomenon requires a deep understanding of flow field. Hence the study of separated flow from bodies and structure has been an active area of research for more than a century.

Solution of the viscous flow over a bluff body has been a challenging problem for a number of years. Such flows are of great interest because they display fundamental fluid dynamic phenomena such as separated shear layers and turbulence. Many structures such as tall buildings, bridges, off-shore pipelines and risers may be considered as bluff bodies and the complex flow over them is of great interest. Also, some streamlined structures may behave as a bluff body at some operating conditions, such as an airplane wing at high angles of attack.

Among the different bluff body shapes, circular section has received considerable attention by researchers. That is partly due to its wide use in many engineering applications (such as pipelines and heat exchanger tubes), partly because of its simple geometry for analysis and simulation, and partly because flow over circular cylinder encompasses all the important aspect of bluff body flow.

When more than one cylinder is placed in a fluid stream, several changes in the characteristics of fluid loads occur due to the interference effect. Investigations of the flow around pair of cylinders can provide a better understanding of the vortex dynamics, pressure distribution and fluid forces, in cases involving more complex

arrangements. The present investigations give a numerical study of the flow about a pair of cylinders in side-by-side arrangement. The main practical application of this investigation is to have a better understanding of the flow around a bundle of risers which links the seabed to the offshore platforms used for oil exploration. These risers are subjected to the shear and oscillatory flows with a very high degree of complexity.

Vortex shedding from bluff bodies can have important consequences from a practical point of view. As the flow field alternates over the body, so does the pressure distribution on the body surface. The alternating pressure distribution results in alternating force components on the body which in turn can cause vibration of an elastic body. Zdravkovich [2, 3] has reviewed the problem of flow interference when two cylinders are placed in side-by-side, tandem and staggered arrangements in a steady flow. It is observed that when more than one bluff body is placed in a fluid flow, the resulting forces and vortex shedding pattern may be completely different from those found on a single body at the same Reynolds number.

Bearman and Wadcock [4] measured the pressure distribution around two cylinders in a side-by-side arrangement, and found a repulsive force between the cylinders for a particular range of gap spacing. For a very small gap, a marked asymmetry in the flow with the two cylinders experiencing different drags and base pressures was observed by them. The drag of two cylinders together was less than the sum of the drags of the isolated cylinders. Williamson [5] experimentally investigated the flow in the Reynolds number range of 150-200 and the gap (L) to diameter (D) ratio of 2.0-6.0. He observed synchronization in vortex shedding and the wakes occurred either in-phase or in anti-phase when L/D exceeded 1.0. For $L/D > 5.0$, the flow around of the cylinders is similar to that encountered for a single circular cylinder.

At an intermediate spacing of L/D = 1.2-2.0, the interaction between the wakes intensifies. The gap flow between the cylinders gets deflected forming one narrow and one wide wake. This phenomenon is called "flopping". The time scale of flopping is more than 1000 times the time scale of vortex shedding. It was found that the frequency associated with narrow wake is almost three times that for the wide wake [4, 6, 7]. The deflected wake may change over from one cylinder to another cylinder intermittently and is bi-stable. The bi-stability is normally independent of Reynolds number [8].

Interactions between vortices in the two wakes lead to the changeover of the gap flow deflection from one side to another. For, $L/D > 2.0$, Wong and Zhou [9] found the flow structure to change from the anti-phase mode to in-phase mode. They also found that for L/D ranging from 1.5 - 2.0, the temporal patterns of C_D and C_L were irregular. For gap to diameter ratio ≥ 2.5, interaction of the wakes became weak, resulting in regular patterns of C_D and C_L for both cylinders.

Surmas et al. [10] investigated the same problem numerically by using lattice Boltzman simulation. They studied two cylinders in tandem and side by side arrangement at Reynolds number of 200. They found that: (i) when the cylinder were aligned along the main-flow direction, vortices are formed at single frequency for Re $\leq$ 200; (ii) transition to turbulence appeared in two dimensional flow, when the cylinders were aligned orthogonal to the main-flow direction and separated by distances smaller than $\approx 2.0D$.

Huang et al. [11] systematically studied the flow around single cylinder, two side-by-side cylinders and one row of cylinders and two rows of cylinders. For flow around one row of cylinders, 180° out of phase vortex shedding was observed when the gap separating the cylinder axes was $4D$ and Reynolds number was 100. Varying the gap between the lateral wall and cylinders triggered the flow to flip from out-of-phase to in-phase vortex shedding. When the gap separating cylinders was less than $2.5D$, the wakes behind the cylinders merged to form clusters and moved in a synchronized in-phase pattern. Ding et al. [12] studied the flow around two circular cylinders arranged in tandem and side-by-side by a mesh free method. They were able to reproduce the various flow regimes observed experimentally.

When the two cylinders were very close to each other ($L/D < 1.2$), the cylinders behave as if they are single cylinder, producing regular patterns of C_D and C_L in time [13]. Based on the sign of average lift coefficient, Lee et al. [13] observed repulsive force between the cylinders. The magnitude of the average repelling force becomes larger as L/D is decreased.

Liang et al. [14] simulated laminar flow past two side-by-side cylinders at various spacing using spectral difference method. As spacing between the cylinders was decreased, single bluff body, flip flopping, anti-symmetric and symmetric wake patterns were predicted. At $L/D = 1.1$, wake flow pattern resembled the vortex street of a single bluff body. At $L/D = 1.4$, 1.5, 1.7 and 2.0, asymmetric flow patterns were predicted and the separation points of the upper and lower cylinders were not synchronized. Anti-symmetric in-phase flow patterns were predicted for arrangements with $L/D = 2.5$ and 3 at Re= 100. When the gap to diameter ratio was increased to 3.4 and 4, the symmetric anti-phase flow patterns were observed.

Kang [15] investigated the flow at Reynolds number ranging from 40-160 and for non-dimensional gap spacing of <5.0. He observed a total of six kinds of wake patterns; anti-phase synchronized, in-phase synchronized, flip flopping, deflected, single bluff body and steady wake patterns. The characteristics of the flow significantly depended on the Reynolds number and gap spacing with the latter much stronger than the former. He observed the bifurcation phenomena where either of two wake patterns can occur at certain flow conditions

Virahsawmy et al. [16] simulated unstable gap flows of three side-by-side cylinders which were equally and unequally spaced. Their simulation in uniform cross flow revealed that the gap flows were unstable and constantly reorienting, which had the effect of restructuring the wake flows behind the cylinders. Chan and Jameson [17] demonstrated by numerical simulation that unsteady vortex wakes generated by side-by-side cylinders can be completely suppressed by counter rotating pair of cylinders. They also reported significant reduction in drag when the cylinder pair was rotated in a doublet-like direction.

The present study is concerned with numerical simulations of two-dimensional, laminar, incompressible, viscous bluff-body flows. The main objectives of present study are as follows:

- To simulate the flow around the two circular cylinders placed in side by side arrangement at Reynolds number of 200 for four values of L/D ratios, namely; $L/D = 1.5$, 2.0, 3.0 and 4.0.

- To find out lift and drag coefficients for each configuration.
- To find out Strouhal number for each configuration.

2. Numerical Simulation

The flow around bluff body in side-by-side arrangement was simulated by using commercial CFD code FLUENT 6.2. The flow problem is solved by continuity and momentum equations in a given domain of interest. The flow is assumed as laminar, two dimensional and unsteady.

The equation for conservation of mass, or continuity equation, can be written as follows

$$\frac{\partial \rho}{\partial t} + \nabla \cdot (\rho \vec{v}) = S_m \tag{1}$$

This equation is the general form of the mass conservation equation and is valid for incompressible as well as compressible flows. The source S_m is the mass added to the continuous phase from the dispersed second phase or from any user-defined sources. In the present study S_m is taken as zero.

A single momentum equation is solved throughout the domain, and the resulting velocity field is shared among the phases. The momentum equation, shown below, is dependent on the volume fractions of all phases through the properties ρ and μ.

$$\frac{\partial}{\partial t}(\rho \vec{v}) + \nabla \cdot (\rho \vec{v} \vec{v}) = -\nabla p + \nabla \cdot \left[\mu\left(\nabla \vec{v} + \nabla \vec{v}^T\right)\right] + \rho \vec{g} + \vec{F} \tag{2}$$

The stress tensor is given by

$$\bar{\bar{\tau}} = \mu\left[\left(\nabla \vec{v} + \nabla \vec{v}^T\right) - \frac{2}{3}\nabla \cdot \vec{v} I\right] \tag{3}$$

where μ is the molecular viscosity, I is the unit tensor, and the second term on the right hand side is the effect of volume dilation.

2.1. Grid generation

The total zero-lift drag coefficient of the body is usually considered to be of three components; friction drag, wave drag, and base drag as shown in Eq. (1). These different components are further discussed in the following sub-sections.

The preprocessor Gambit is used to generate two-dimensional Cartesian grid. The computational domain is discretized using quadrilateral structured meshes. Finite volume method is used to solve the Navier-Stokes equations representing the flow field. Fine cells are used near the cylinder surface whereas coarser cells are adopted near the wall boundary. The closest mesh point in the normal direction to the cylinder surface is located at a distance around $0.005D$. The mesh point distributions are concentrated near the cylinder wall in order to give more accurate boundary-layer solution.

A typical computational quadrilateral mesh is shown in Fig. 1. The figure refers to L/D = 3.0, where L is the distance between the centres of the cylinders and D is the diameter of the cylinder. The computational mesh for this case consists of 20,000 cells. Figure 2 shows a detail of the mesh near the cylinder walls, stressing the importance of a suitably concentrated nodal distribution in the boundary layer. The number of cells for other L/D ratios is slightly different, but the characteristics of the meshes are essentially the same.

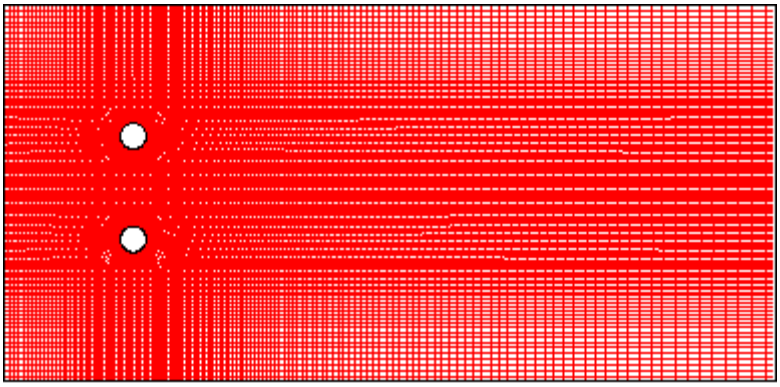

Fig. 1. Quadrilateral Mesh for Side–by-Side Arrangement.

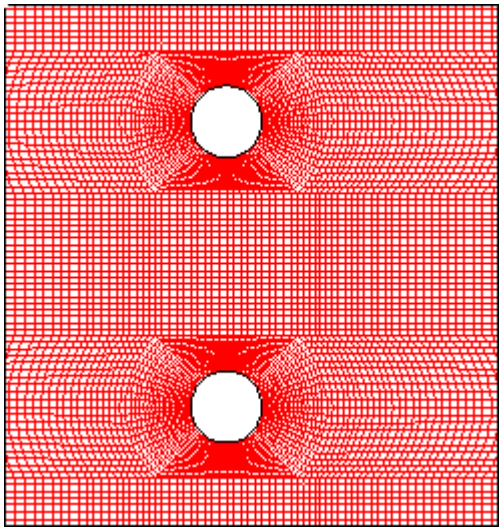

Fig. 2. Detail of Mesh near the Walls of Both Cylinders.

2.2. Model prediction

The flow field around the cylinders is modeled in two-dimensions with the axis of the cylinder perpendicular to the direction of flow. The cylinder is modeled as a

circle and a rectangular flow domain is created around the cylinder. A uniform velocity at the inlet of the flow domain is specified.

The value of the free stream velocity employed in the present investigations, U_o = 0.01005 m/s and is based on Reynolds number of 200 with a cylinder diameter of 20 mm. The outer boundary of the mesh extends downstream to 25.5*D* and upstream to 7.5*D*, Fig. 3(a). In the vertical direction, the outer boundaries are located at -7.5*D* and 7.5*D*. The point with coordinate (0, 0) is located between two cylinders. The time step used for the unsteady simulation is calculated using the equation

$$\mathrm{St} = 0.2 = \frac{fD}{U_o} \tag{4}$$

where St is Strouhal number, *f* is vortex shedding frequency. The Strouhal number for flow past cylinder is roughly 0.2. The time step thus obtained is 0.398 seconds. In order to capture the shedding correctly, at least 20 to 25 time steps are required in one shedding cycle. Simulation was run for around 1200 time steps for all the cases.

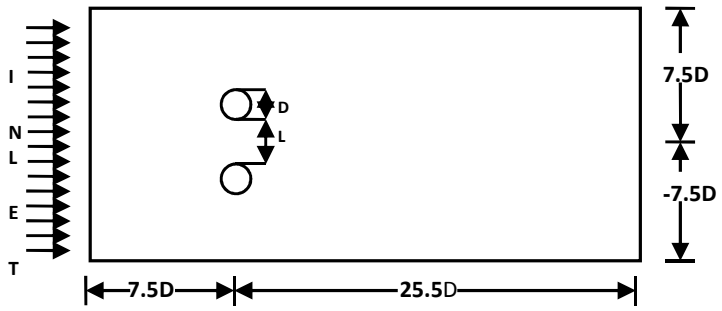

Fig. 3(a) Simulation Domain for the Fluid Flow against Two Cylinders Orthogonal to the Main Flow. Distance *L* between the Centres of Two Cylinders is varied from 1.5*D* to 4*D*.

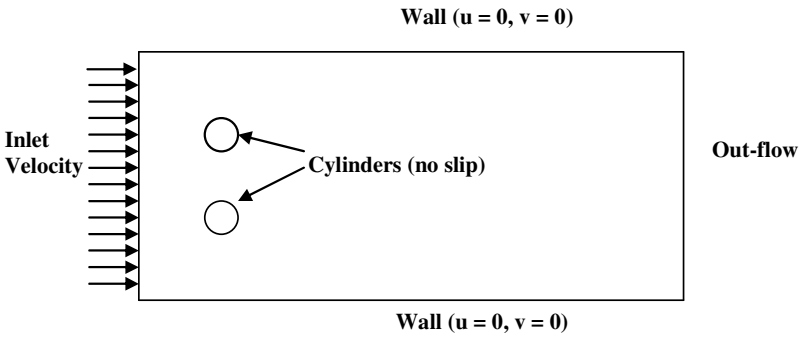

Fig. 3(b) Boundary Condition for Side-by-Side Arrangement.

The computational domain with boundary conditions is shown in the Fig. 3(b). At the inlet of flow domain velocity boundary condition is used. As the velocity and pressure distribution at the outlet are not known, outflow boundary condition is used. The values for all the variables are obtained by extrapolation from the interior. No slip condition is imposed on the wall and cylinders. Final convergence is decided by the way of a residual source criterion, which measures the departure from exactness for all the flow variables. The convergence criterion was set as less than 1×10^{-6} for the normalized total overall residue of all variables. Grid independency is performed for 20,000 and 40,000 number of cells and it is found that variation in drag force, lift force and Strouhal number are less than one percent. Hence computations were carried out with around 20,000 cells.

3. Results and Discussion

3.1. Lift and drag coefficients

The instantaneous variation lifts and drag coefficients obtained for various *L*/*D* ratios are presented in Figs. 4-7. The lift and drag coefficients are defined as

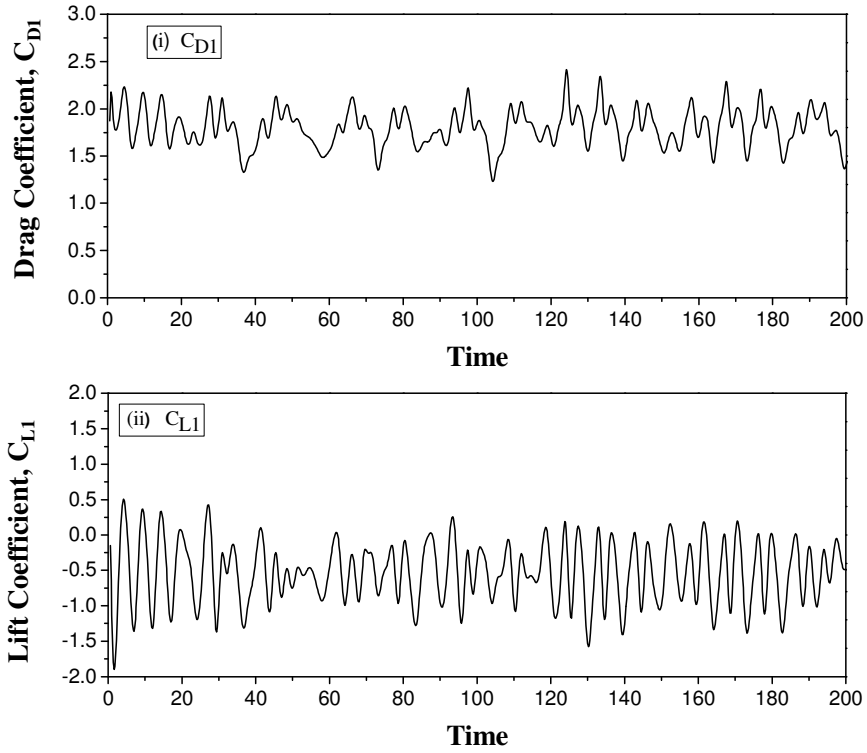

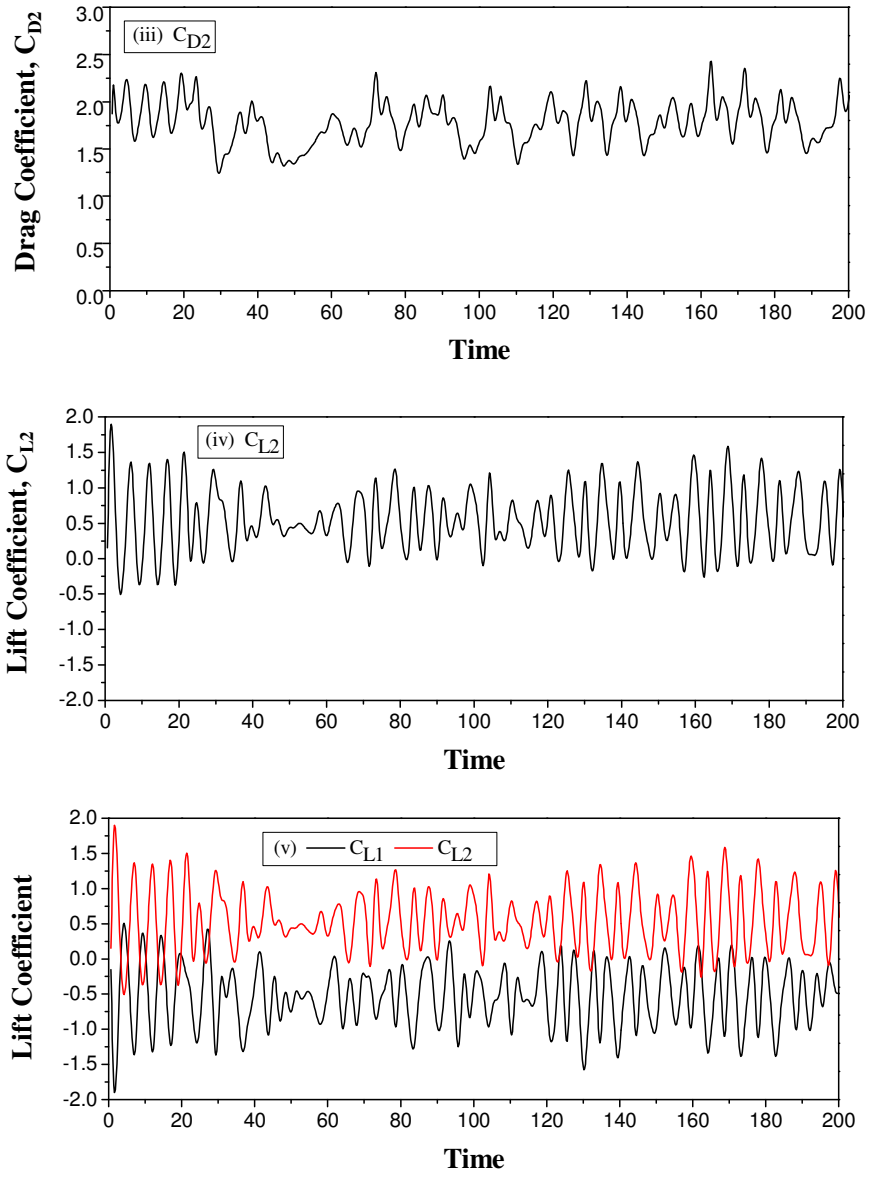

Fig. 4(a) Variation of Drag and Lift Coefficients with Time for *L/D* = 1.5.

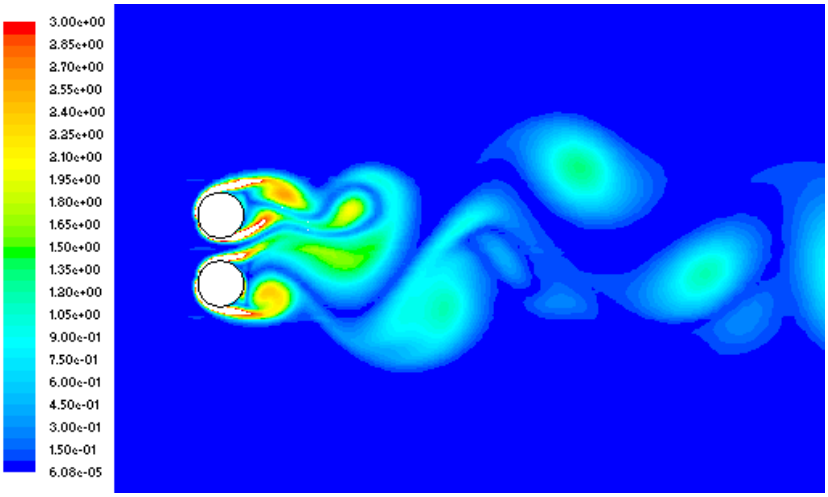

Fig. 4(b) Contour of Vorticity Magnitude for *L/D* = 1.5.

$$C_L = \frac{L}{\frac{\rho}{2} U_o^2 A} \tag{5}$$

$$C_D = \frac{D}{\frac{\rho}{2} U_o^2 A} \tag{6}$$

Figs 4-7 show the time variation of the lift and drag coefficients for *L/D* = 1.5, 2.0, 3.0 and 4.0 respectively. In the panel (i) of Fig. 4(a), the time history of the drag force for *L/D* = 1.5 can be seen. For this case there is repulsive force acting on the cylinders, in accordance with the results observed experimentally [4, 5]. The average lift coefficient of the upper cylinder is positive and that for the lower cylinder is negative, (panels (ii) and (iv)).

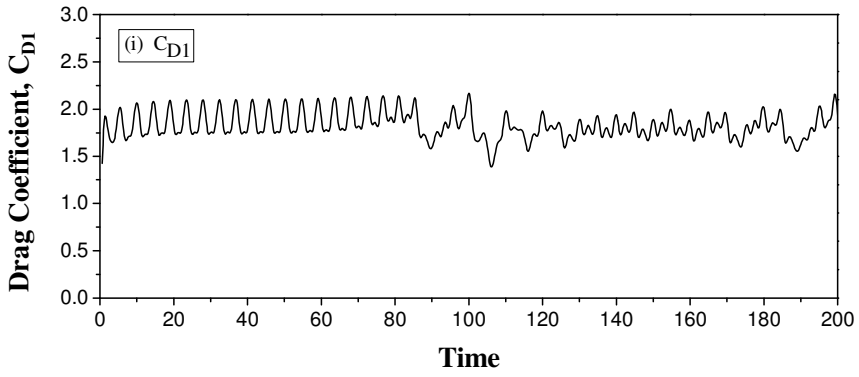

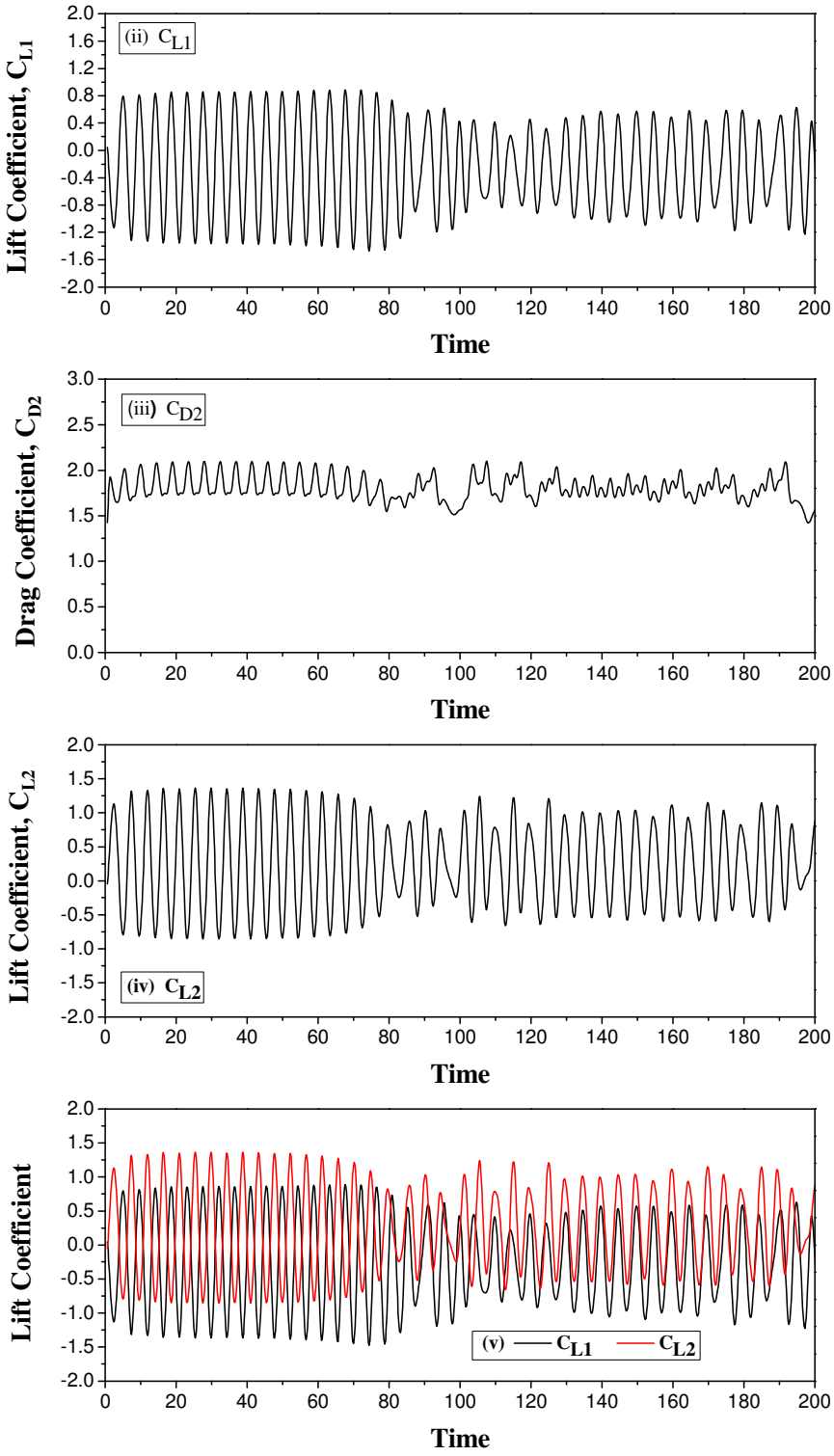

Fig. 5(a) Variation of Drag and Lift Coefficients with Time for *L/D* = 2.0.

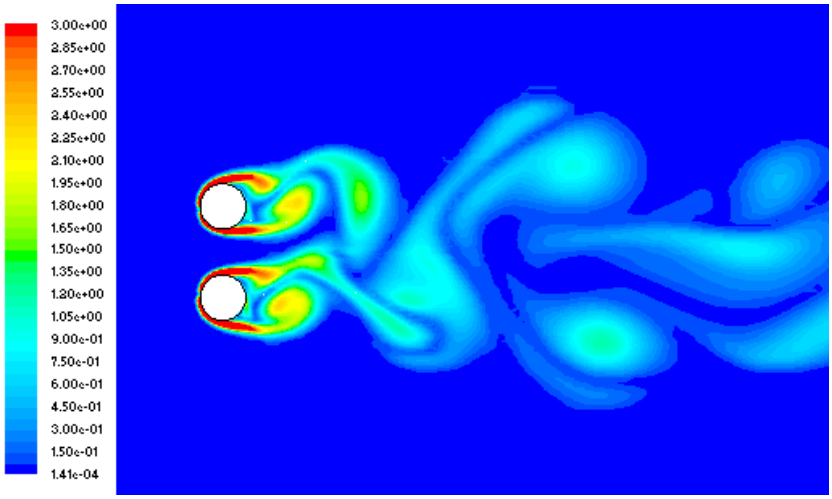

Fig. 5(b) Contour of Vorticity Magnitude for *L/D* = 2.0.

The lift coefficient is defined as positive in the upward direction for the upper cylinder and negative for the lower cylinder. As the flow approaches the cylinders, a region of high pressure forms in front of the cylinders. Though the pressure drop occurs in the gap between the cylinders, the pressure will still be higher than the pressure at both opposite sides of the cylinders. The frontal stagnation points move in the direction of the gap, (Figs. 11-14). The positions of the separation points in the lower and upper cylinders seem to be moving in clockwise and anti-clockwise directions respectively. The net result of this pressure field is to cause a repulsive force between the cylinders.

For *L/D* ratio $\leq$ 2.0, the interaction between the wakes associated with two cylinders is expected to intensify. The gap flow between the cylinders is deflected, forming one narrow and one wide wake, (Figs. 4(b) and Fig. 11)). In the above figures the upper cylinder is associated with narrow wake and lower cylinder with wide wake. The deflected gap flow may change intermittently from one side to another and is bi-stable. Bearmann and Wadcock [4] and Williamson [5] observed in their experiments that the biased flow pattern is bi-stable, i.e., the narrow and wide wakes, and the direction of the gap flow switch from one cylinder to the other. The vertical structures in the wide wake start to occur at a greater downstream distance. On the other hand, those in the narrow wake, the vertical structures visible at much closer position, (Fig.11).

At a larger distance, the two streets appear merging into one. Vortical structures in the narrow wake behave differentially from those in the wide wake. The frequency associated with the narrow wake is higher than that associated the wide wake [6, 8, 18].

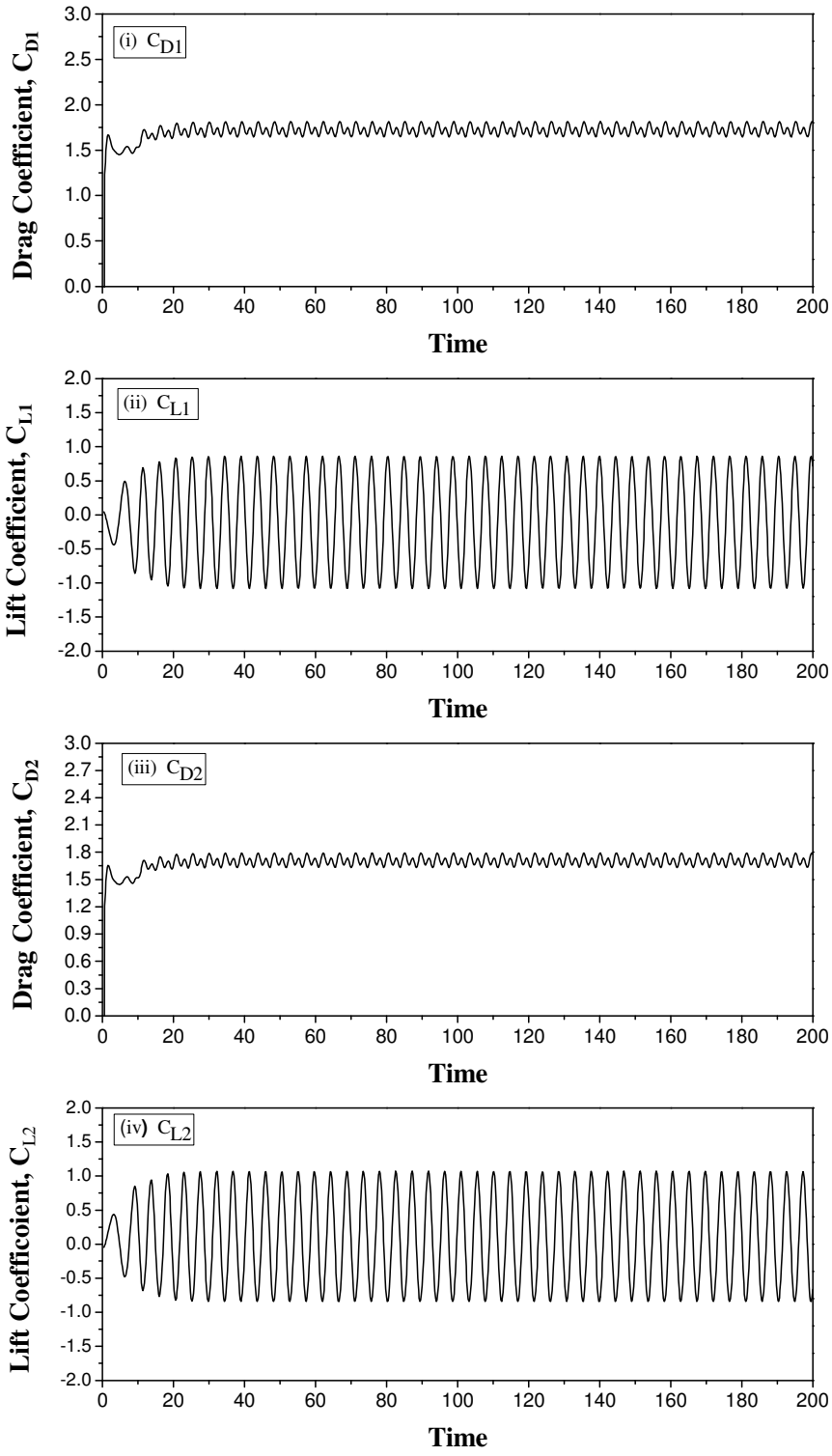
(i) C_{D1}
Drag Coefficient, C_{D1}
Time
(ii) C_{L1}
Lift Coefficient, C_{L1}
Time
(iii) C_{D2}
Drag Coefficient, C_{D2}
Time
(iv) C_{L2}
Lift Coefficoient, C_{L2}
Time

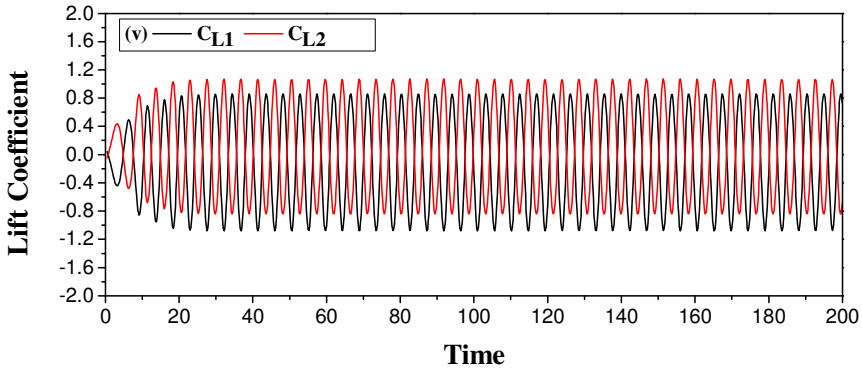

Fig. 6(a) Variation of Drag and Lift Coefficients with Time for *L/D* = 3.0.

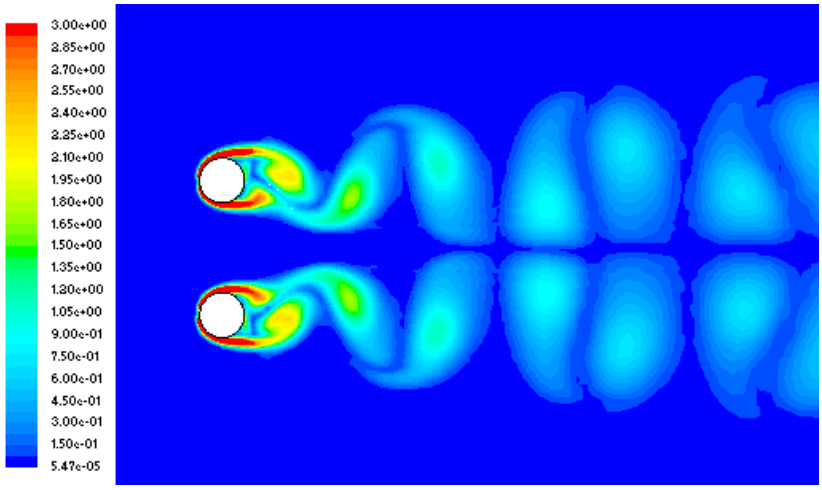

Fig. 6(b) Contour of Vorticity Magnitude for *L/D* = 3.0.

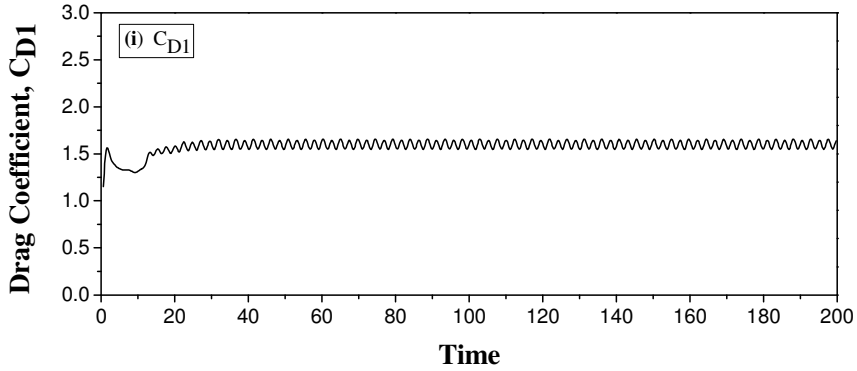

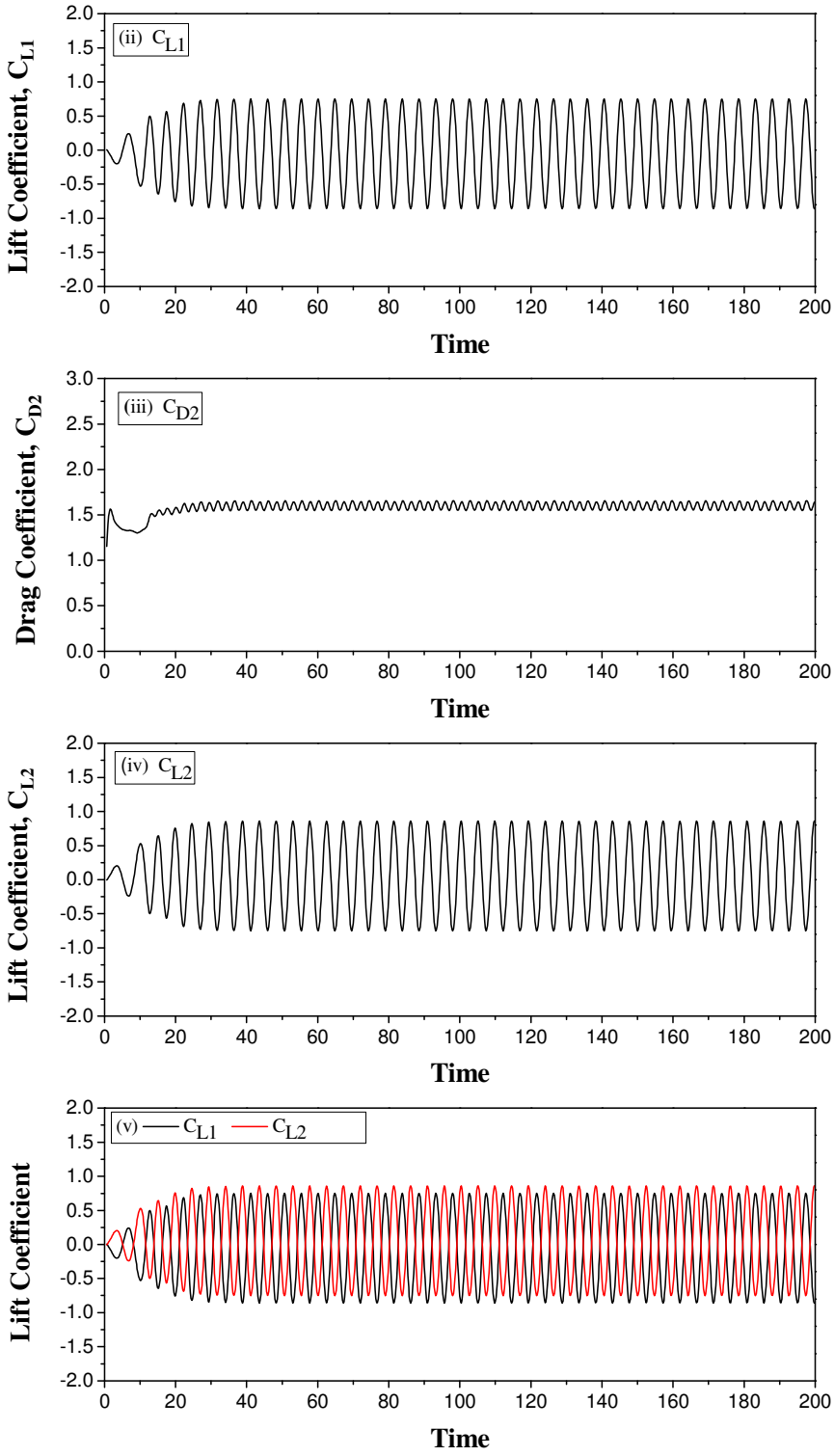

Fig. 7(a) Variation of Drag and Lift Coefficients with Time for *L/D* = 4.0.

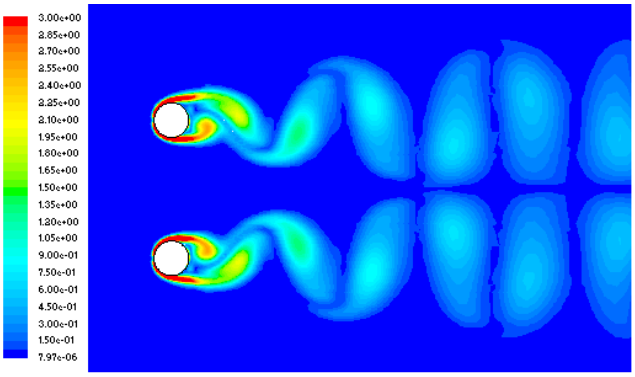

Fig. 7(b) Contour of Vorticity Magnitude for *L/D* = 4.0.

As the wake is deflected towards one of the cylinders its drag increases. Wake and its consequent pressure difference are responsible for the creation of drag. Hence deflected wake causes increase in drag coefficient. However, the flopping observed experimentally has a time scale considerably higher than the one observed in the present simulation. Also observed that the wake was deflected towards one of the cylinders and it remained deflected during several cycles of vortex shedding [8]. The main reason for this disagreement could be that the Reynolds number in the present simulation is lower than that of [8] and the flow is treated as two dimensional.

The results for *L/D* = 2.0 are shown in Fig. 5. The flopping phenomenon can still be seen in the drag time history, (panels (i) and (iii), Fig. 5(a)). The vorticity and streamline contours for this gap are shown in Fig. 5(b). The repulsive force between the cylinders is diminished, but the wake still resembles the wake of asingle body. For this spacing the wake is clearly not organized, with the time histories of the force coefficients indicating only the net effect of repulsion between the cylinders. The lift coefficient is in anti-phase initially up to non-dimensional time of about 80 and then the lift coefficient exhibits in-phase tendency and is asymmetric, (panels (ii), (iv)) and (v), Fig. 5(a)). Wong and Zhou [9] also found the flow structure to change from the ani-phase mode to in-phase mode. The mode change from anti-phase to in-phase as observed for *L/D* = 2.0 and vice-versa is not fully understood.

At *L/D* = 3.0, the flopping vanishes. It is observed in Fig. 6(a) that the drag coefficients for both cylinders are the same. There is a synchronization of the lift from the upper and lower cylinders with a phase of about 180^{o}, corroborating the anti-phase wake visualization, (panel (v), Fig. 6(b)). This is also experimentally wakes in anti-phase for this *L/D* ratio [4, 5]. The wakes behind each cylinder are symmetrical. Figure 6(a) panel (v) clearly indicates the anti-phase mode. This behaviour is also observed for *L/D* = 4.0 as is seen in Fig. 7. For higher values of the gap, the repulsion force between the cylinders diminishes, suggesting that the isolated cylinder result is recovered.

Relatively stable anti-phase vortex shedding is likely attributed to a possibly symmetric pressure differentiation about the centre line. The pressure

measurement around two cylinders by Zhou et al. [19] indicated that the pressure upstream of the gap between the cylinders was higher than that close to the free stream because of flow retardation. They inferred that there was a pressure differentiation on the two sides of each cylinder in the cross flow direction. The differentiation may be symmetrical with respect to $y/D = 0$, as supported by the numerical calculation of the pressure field around two side-by-side cylinders at $L/D = 3$ and 4 [20]. Such a pressure distribution is likely to suppress in-phase vortex shedding and induce anti-phase behavior.

At $L/D = 3$ and 4, Figs. 6(b) and 7(b) indicate that the ant-phase vortex shedding forms two parallel anti-phase streets that are symmetric with respect to the centre line. The flow preserves its structure very far downstream without any distortion which agrees with the experimental studies of [5 and 19].

At higher L/D ratios, the merging process becomes less active due to the weaker mutual interaction between the two single cylinder wakes. The flow did not attain single vortex street for $L/D = 3.0$ and 4.0. On the other, for $L/D = 1.5$ and 2.0, the merging process becomes more active due to the closer proximity of two cylinders.

Table 1. Average Drag Coefficient and Strouhal Number for Side-by-Side Arrangement.

Gap L/D	C_{D1}	C_{D2}	C_{L1}	C_{L2}	St_1	St_2
1.5	1.782	1.782	0.540	-0.540	0.209	0.209
2.0	1.792	1.792	0.238	-0.238	0.200	0.200
3.0	1.701	1.701	0.095	-0.095	0.217	0.217
4.0	1.602	1.602	0.0500	-0.050	0.213	0.213

Fourier analysis of the lift coefficient on the upper cylinder, for the ratios $L/D = 1.5$, 2.0, 3.0, and 4.0, is shown in Fig. 8. In this figure the abscissa represents the Strouhal number and the power-spectrum is shown in 'y' axis. It is interesting to notice that for the cases where the $L/D = 1.5$ and 2.0, the spectra are broad-banded with a peak, not particularly sharp located at St = 0.21. For these gaps the "flopping" phenomenon has been observed and the wakes are not synchronized. The characteristics of the spectra observed are in agreement with the random nature of the lift results shown in Figs. 4 and 5. As the ratio is increased to $L/D = 3$, the wakes forming from the two cylinders become synchronized and is shown in Fig. 8(c). The spectrum shows a very distinctive peak at St = 0.21.

The average lift and drag coefficients, Strouhal number are presented in Table 1. Analyzing this table, it is concluded that as the L/D increases from 1.5 to 2 the drag coefficient slightly increases. The drag coefficient on either cylinder begins to fall for ratios $L/D > 2.0$.

When the cylinders are in close proximity, the pressure distribution on the upper and lower portions of each cylinder will not be uniform, thus generating lift force in opposite direction. The drag is generated due to the difference in pressure in the direction of the flow. At $L/D = 2.0$, flopping of the flow was observed with narrow and wide wakes. Hence, the drag coefficient of the cylinders at this gap ratio is slightly higher. As the gap ratio is increased the fluid between the cylinders goes through the gap without getting deflected. With the result, the pressure difference

across the cylinder reduces thus reducing the drag force. From Table 1, it can also be observed that the values of lift and drag coefficients are reducing as *L*/*D* ratio is increased. The flow interference effect decreases as the cylinders are moved apart. It could be interpreted that for very large *L*/*D* ratios, values will approach that of an isolated cylinder. The results agree closely with [4], [10] and [19].

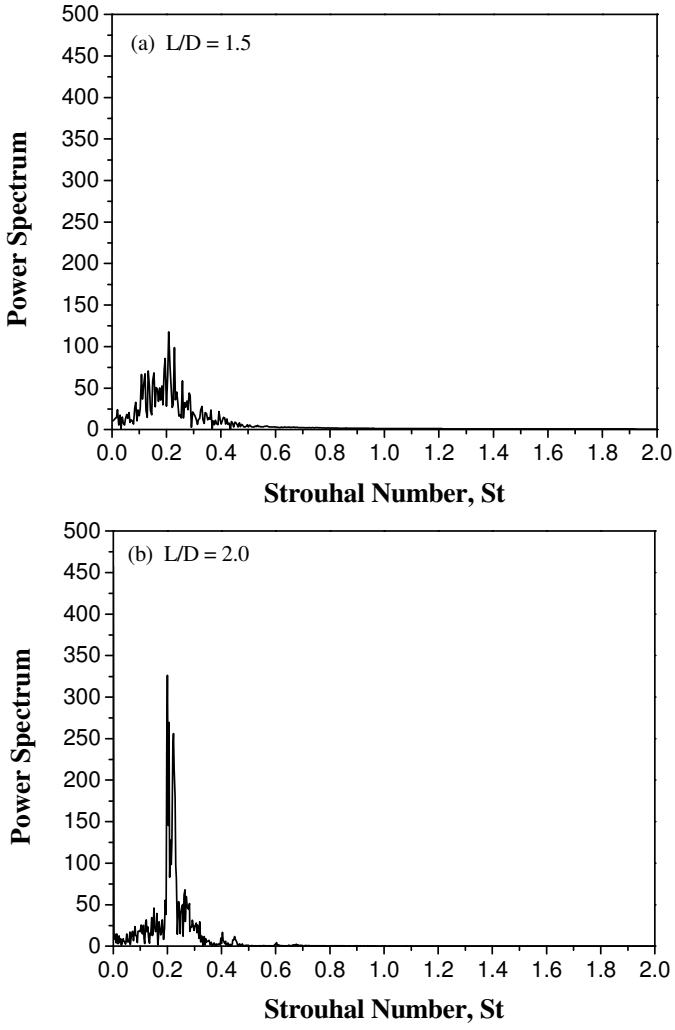

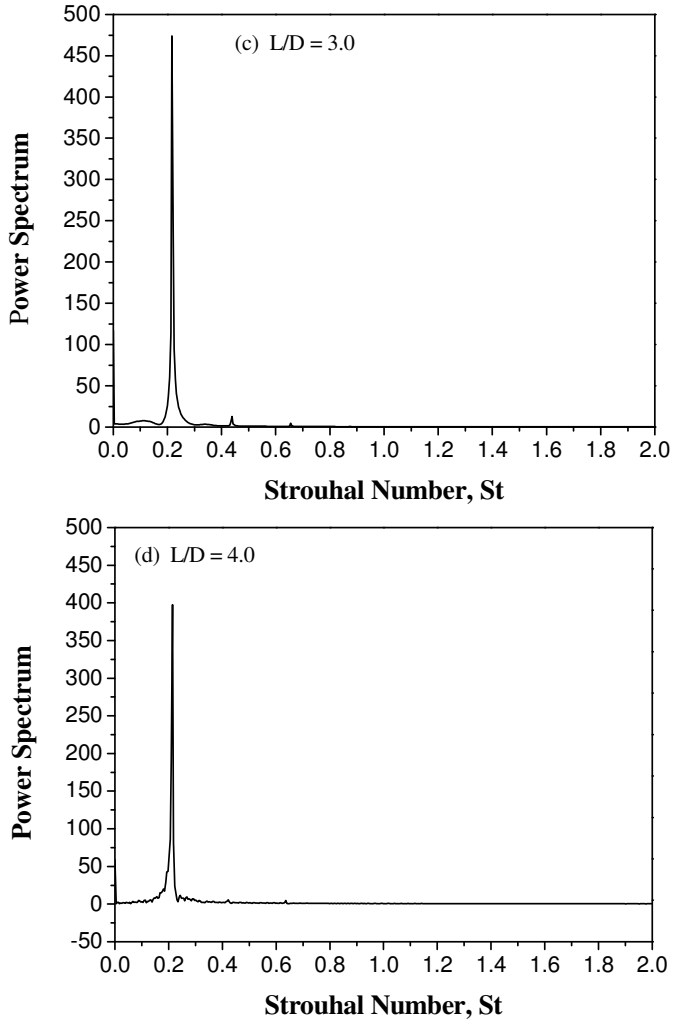

Fig. 8. Power Spectrum of the Lift Coefficient against Strouhal Number (a) *L/D* = 1.5, (b) *L/D* = 2.0, (c) *L/D* = 3.0, (d) *L/D* = 4.0.

Figures 9 and 10 compare the present results with that obtained by Surmas et al. [10] who have used lattice Boltzmann simulation. Figure 9 shows that Surmas et al. [10] calculations predict almost the same drag coefficient for each gaps value. Drag coefficient for present result are slightly more than Surmas et al. [10] results. But this difference in drag coefficient decreases as the gap between two cylinders is increased. The agreement between present and Surmas et al. [10] results can be considered good for the lift coefficient (Fig. 10).

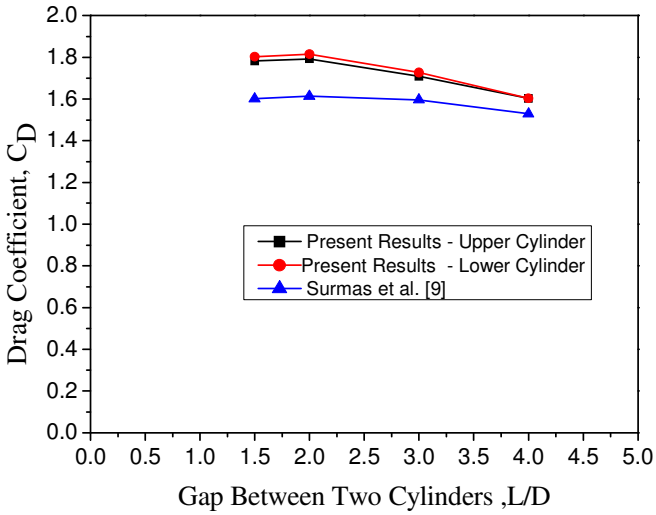

Fig. 9. Drag Coefficient on the Two Cylinders at Re = 200.

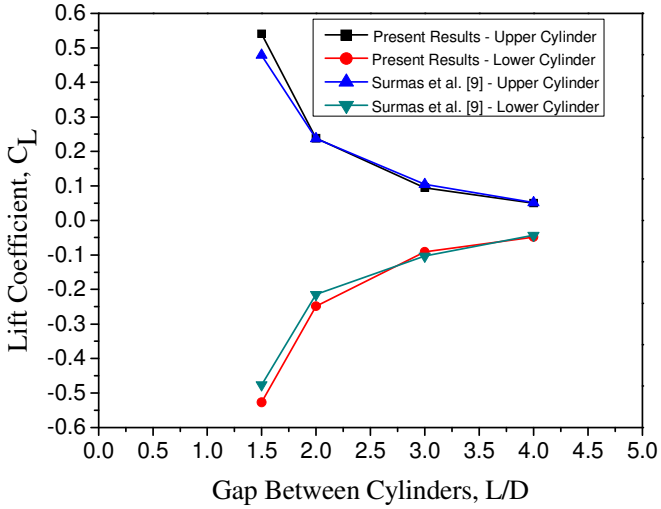

Fig. 10. Lift Coefficient on the Two Cylinders at Re = 200.

3.2. Wake structure

When fluid flows over a bluff body, the boundary layer typically separates from the surface and the separation occurs near the maximum width of the body or at a sharp corner. The separated flow forms shear layers on both sides of the body. There is a velocity gradient across the shear layers, since the outer portion of each shear layer in contact with the free-stream moves faster than its inner portion that was in contact with the body surface. Hence the shear layers roll up and form two opposite-rotating vortices behind the body [21].

The shear layers however can become unstable due to natural disturbances in the flow and trigger one of the vortices to grow faster than the other. The larger

vortex grows so much that it draws the opposite shear layer across the near wake. This vortex is then released from the body and is convected downstream in the wake. Then, in the absence of the first vortex the other vortex on the opposite side grows faster while the shear layer on the first side rolls up and forms a new vortex [22]. This process continues and a "street" of vortices will appear in the wake of the body. The vortices in the wake diffuse as they move further downstream and at large distances from the body coalesce into each other and eventually fade out.

The wake structures for different gap values are shown in Figs. 11-14. For L/D = 1.5 vortices are formed behind both cylinders as shown in Fig 11. When the lower cylinder vortices are detached and upper cylinder vortices are attached, the jet like fluid flows towards upper cylinder. When the vortices are shed, flow issues like jet in passage between the cylinders, creating an intensive mixing action with the main fluid. When L/D = 2.0, the vortices are formed at the top and bottom of upper and lower cylinder respectively, Fig. 12.

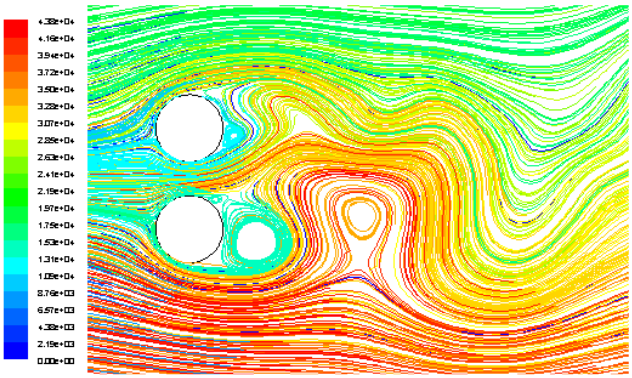

Fig. 11. Wake Structure for L/D = 1.5.

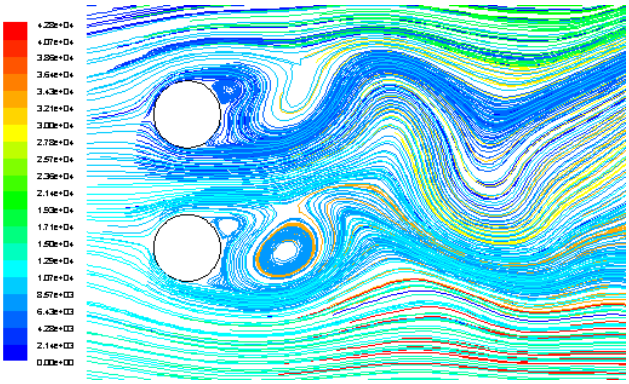

Fig. 12. Wake Structure for L/D = 2.0.

Figure 13 shows the wake structure for L/D = 3.0. For this configuration, vortices are formed at the bottom and top of the upper and lower cylinder respectively. The flow between the cylinders is almost straight. When gape is increased to L/D = 4.0, the cylinder no longer influence each other, Fig.14. Vortices are formed and shed alternatively. As the cylinders are far apart, they do

not influence the fluid passing between them. The inner vortices separate but do not influence each other, with the result, the fluid between the cylinders goes without getting deflected.

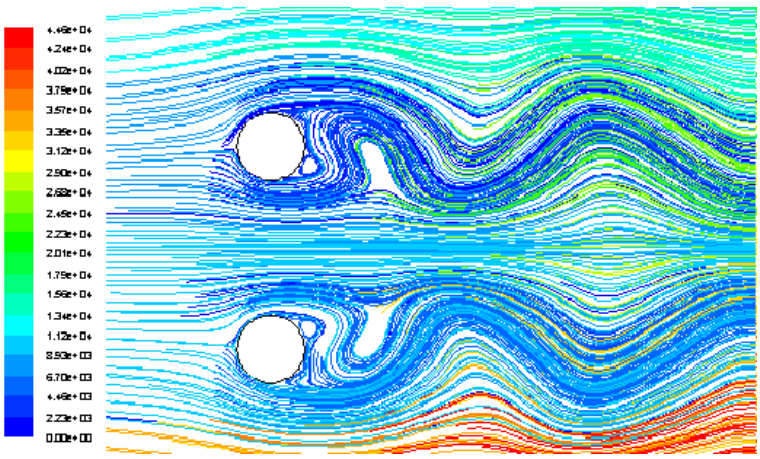

Fig. 13. Wake Structure for *L/D* = 3.0.

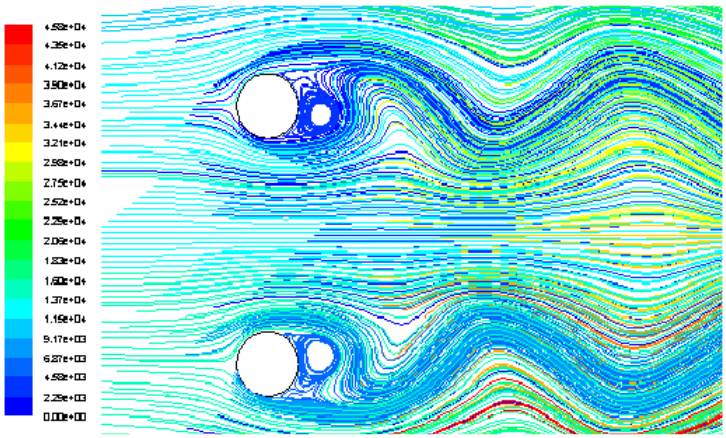

Fig. 14. Wake Structure for *L/D* = 4.0.

4. Conclusions

In the present investigation, the flow around bluff body in side-by-side arrangement for Reynolds number of 200 is simulated. Vorticity contours and variation of lift and drag coefficients with time are presented.

A force between the cylinders which is repulsive in nature is observed. This repulsive force reduces as *L*/*D* ratio is increased. Also, a "flopping" phenomenon is observed for $L/D \leq 2.0$. However, the time scale is considerably shorter than that observed by Kim & Durbin [8]. The drag coefficient for $L/D = 2$ is slightly higher than for other *L*/*D* ratios. Beyond this ratio, the drag coefficient falls. The

lift coefficient decreases with increase in *L/D* ratio. For *L/D* = 3.0 and 4.0, the power spectrum estimation of the lift coefficient shows a very distinctive peak at Strouhal number of 0.21. For these gap ratios, both cylinders shed synchronized vortices and are in anti-phase.

References

1. Billah, K.Y.; and Scanlan, R.H. (1992). Resonance, Tacoma narrows bridge failure and undergraduate physics. *American Journal of Physics*, 59(2), 118-124.
2. Zdravkovich, M.M. (1977). Review of flow interference between two circular cylinders in various arrangements. *ASME Journal of Fluids Engineering*, 99(4), 618-633.
3. Zdravkovich, M.M. (1987). The effects of interference between circular cylinders in cross flow. *Journal of Fluids and Structures*, 1(2), 239-261.
4. Bearman, P.W.; and Wadcock, A.J. (1973). The interaction between a pair of circular cylinders normal to a stream. *Journal of Fluid Mechanics*, 61(3), 499-511.
5. Williamson, C.H.K. (1985). Evolution of a single wake behind a pair of bluff bodies. *Journal of Fluid Mechanics*, 159, 1-18.
6. Sumner, D.; Wong, S.S.T.; Price, S.J.; and Païdoussis, M.P. (1999). Fluid behavior of side-by-side circular cylinders in steady cross flow. *Journal of Fluids and Structures*, 13(3), 309-338.
7. Sumner, D.; Price, S.J.; and Doussis, M.P. (1998). Investigation of side-by-side circular cylinders in steady cross-flow by particle image velocimetry. *Proceedings 1988, ASME Fluids Engineering*, *Division Summer Meeting*, Paper 37.
8. Kim H.J. (1988). Investigation of the flow between a pair of cylinders in the flopping regime. *Journal of Fluid Mechanics*, 196, 431-448.
9. Wang, Z.J.; and Zhou, Y. (2005). Vortex interaction in a two side-by-side cylinder near-wake. *International Journal of Heat and Fluid Flow*, 26(3), 362-377.
10. Surmas, R.; dos Santas, L.O.E.; and Philippi, P.C. (2004). Lattice Boltzmann simulation of the flow interference in bluff body wakes. *Future Generation Computer Systems*, 20(6), 951-958.
11. Huang, Z.; Olson, J.A.; Kerekes, R.J.; and Green, S.I. (2006). Numerical simulation of the flow around rows of cylinders. *Computers & Fluids*, 35(5), 485-491.
12. Ding, H.; Shu, C.: Yeo, K.S.: and Xu, D. (2007). Numerical simulation of flows around two circular cylinders by mesh-free least square based finite difference methods. *International Journal for Numerical Methods in Fluids*, 53(2), 305-332.
13. Lee, K.; Yang, K.S.; and Yoon, D.H. (2009). Flow induced forces on two circular cylinders in proximity. *Computers & Fluids*, 38(1), 111-120.
14. Liang, C.; Premasuthan, S.; and Jameson, A. (2009). High-order accurate simulation of low-Mach laminar flow past two side-by-side cylinders using spectral difference method. *Computers & structures*, 87(11-12), 812-827.

15. Kang, S. (2003). Characteristics of flow over two circular cylinders in a side-by-side arrangement at low Reynolds numbers. *Journal of Physics of Fluids,* 15(9), 2486-2498.
16. Chen, L.; Tu, J.; Zhou, Y.; Virahsawmy, H.; and MacGillivray, I. (2005). Computation of flow behind three side-by-side cylinders of unequal/equal spacing. *Australian and New Zealand Industrial and Applied Mathematics*, 46, 672-689.
17. Chan, A.S.; and Jameson, A. (2010). Suppression of the unsteady vortex wakes of a circular cylinder pair by a doublet-like counter-rotation. *International Journal for Numerical Methods in Fluids*, 63(1), 22-39.
18. Ishigai, S.; Nishikawa, E.; Nishimura, K.; and Cho, K. (1972). Experimental study on structure of gas flow in tube banks with tube axes normal to flow (part 1, Karman vortex flow around two tubes at various spacings). *Bulletin of the JSME*, 15, 949-956.
19. Zhou, Y.; Wang, Z.J.; So, R.M.C.; Xu, S.J.; and Jin, W. (2001). Free vibrations of two side-by-side cylinders in a cross flow. *Journal of Fluid Mechanics*, 443, 197-229.
20. Meneghini, J.R.; and Saltara, F., Siqueira, C.L.R.; and Ferrari Jr., J.A. (2001). Numerical simulation of flow interference between two circular cylinders in tandem and side-by-side arrangement. *Journal of Fluids and Structures,* 15(2), 327-350.
21. Williamson, C.H.K.; and Roshko, A. (1988). Vortex formation in the wake of an oscillating cylinder. *Journal of Fluids and Structures*, 2(4), 355-381.
22. Gerrard, J.H. (1966). The mechanics of the formation region of vortices behind bluff bodies. *Journal of Fluid Mechanics*, 25(2), 401-413.